Heat energy balance in the convective atmospheric boundary layer at Xianghe (Beijing Area), China

Heat Energy Balance in the Convective Atmospheric Boundary Layer at Xianghe (Beijing Area), China

M. W. QIAN

LAPC, Institute of Atmospheric Physics, Chinese Academy of Sciences, Beijing, China, and CCSEM-World Laboratory, Lausanne, Switzerland

A. LONGHETTO

Dipartimento di Fisica Generale, Universita' Degli Studi di Torino, Torino, Italy, and CCSEM-World Laboratory, Lausanne, Switzerland

C. CASSARDO

Dipartimento di Scienze e Tecnologie Avanzate, Universita' di Alessandria, Alessandria, Italy

C. GIRAUD

Istituto di Cosmogeofisica del CNR, Torino, Italy, and CCSEM-World Laboratory, Lausanne, Switzerland

Z. X. HONG, W. D. LUO, AND Y. J. ZHAO

LAPC, Institute of Atmospheric Physics, Chinese Academy of Sciences, Beijing, China, and CCSEM-World Laboratory, Lausanne, Switzerland

(Manuscript received 7 May 1999, in final form 29 March 2000)

ABSTRACT

A simple and physically consistent expression for the turbulent heat flux equation in the convective atmospheric boundary layer (CABL) has been suggested by Holtslag and Moeng in 1991. In their equation, valid under quasi-steady states and horizontal homogeneity, the countergradient term resulted from the third-moment transport effect rather than from the buoyancy production term. In this paper, experimental observation data from the World Laboratory Applied Research Project on Drought and Desertification (WL-ARPDD94 Experiment), carried out in a flat region of the greater Beijing area, China, have been utilized with the purpose of checking the validity of the Holtslag and Moeng equation. The result of this experimental check proved to be more than satisfactory through most of the CABL.

1. Introduction

It has long been recognized that the upward transport of heat in the upper regions of the convective atmospheric boundary layer (CABL) can hardly be described in terms of *K* theories based on local gradient of potential temperature (Deardorff 1966, 1972; Ebert et al. 1989).

The reason is that the potential temperature gradient is relatively small in the CABL, and what is more, in its upper half it even shows slightly stable positive values that cause the transport to be countergradient (Deardorff 1972; Holtslag and Moeng 1991; Wyngaard and Weil 1991; Cuijpers and Holtslag 1998; Zilitinkevich et al. 1999).

Among the many attempts to deal with nonlocal countergradient transport, we recall here the pioneer work made by Deardorff in 1972 and the more recent studies of Holtslag and Moeng in 1991 and Zilitinkevich et al. in 1999. The first two approaches introduce a countergradient term in a simplified heat flux equation, but they are substantially different as far as the physical derivation of this term and its interpretation are concerned. In fact, Deardorff (1972) derived the countergradient term from the buoyancy production term of the equation for the heat flux, while Holtslag and Moeng (1991) ob-

Corresponding author address: Prof. A. Longhetto, Dipartimento di Fisica Generale, Universita' Degli Studi di Torino, Via Pietro Giuria, 1, 10125 Torino, Italy.
E-mail: longhetto@ph.unito.it

tained the countergradient term from the buoyancy production term and parameterized it in terms of nonlocal convective velocity and temperature scales (θ_* and w_*).

The third approach (Zilitinkevich et al. 1999) is an advanced nonlocal turbulence closure scheme providing an improved ''turbulence advection plus diffusion parameterization'' of the third-order transport term in the budget equation for the turbulence heat flux in the CABL.

In our paper, we turn in particular our attention to the derivation of Holtslag and Moeng (1991), whose parameterization of the countergradient term seemed to us to be a very interesting and physically consistent generalization of previous proposals (for instance, Troen and Mahrt 1986), with the addition of simplicity, which makes it particularly suited for practical applications in atmospheric and diffusion models.

However, as the derivation of the countergradient term made by Holtslag and Moeng is largely based on large eddy simulation (LES) data (Moeng and Wyngaard 1986, 1989), a validation of its main assumptions against field observations of turbulence and mean vertical profiles in the CABL still seems to be appropriate.

In this paper, a comparison between the terms of the Holtslag and Moeng simplified version of the heat flux equation (section 2) and the corresponding ones resulting from observation in a field experiment is performed. The experiment, described in section 3, was carried out in Xianghe (southeast of Beijing), China, in August–September 1994, in the frame of the World Laboratory Applied Research Project on Drought and Desertification (WL-ARPDD94 Experiment). The results of the field experiment are discussed in sections 4 and 5, while in section 6 we present the results of their comparison with the Holtslag and Moeng derivation.

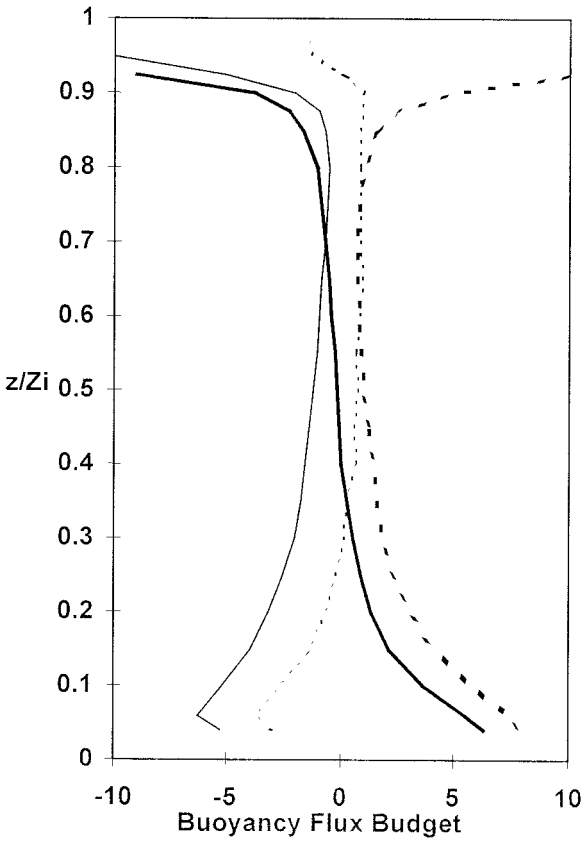

FIG. 1. The normalized terms (by $w_*^2\theta_*/Z_i$) at the rhs of the heat flux equation (1), as a function of relative height [adopted from Holtslag and Moeng (1991) and Moeng and Wyngaard (1989)]. Thin solid line represents P, thin dash line T, thick solid line M, and thick dash line B.

2. Countergradient transport of heat

Without going into unnecessary details, we recall the turbulent heat flux equation under the assumption of horizontal homogeneity and with the Boussinesq approximation (Deardorff 1972):

$$\frac{\partial\overline{w\theta}}{\partial t} = -\frac{\partial\overline{w^2\theta}}{\partial z} - \overline{w^2}\frac{\partial\Theta}{\partial z} + \frac{g}{\Theta}\overline{\theta^2} - \frac{1}{\rho_0}\overline{\theta\frac{\partial p}{\partial z}}, \quad (1)$$

(T) (M) (B) (P)

where ρ_0 is the reference density of air; Θ is the average potential temperature; w and θ are the fluctuations of vertical velocity and temperature, respectively; $\overline{w\theta}$ is the turbulent heat flux; and p is the pressure fluctuation. The terms on the right-hand side of the above equation are, in order, the turbulent transport (T), the mean gradient production (M), the buoyant production (B) and the pressure covariance (P). Bars over cross products of fluctuating quantities represent correlation products and are time averaged.

From Eq. (1), Holtslag and Moeng (1991) derived the countergradient term by utilizing the results of large eddy simulation, from which they found that the transport term (T) of the heat flux equation is not negligible when compared with other terms. The vertical profiles in the CABL of the normalized terms at the rhs of Eq. (1) are shown in Fig. 1, taken from the papers of Holtslag and Moeng (1991) and Moeng and Wyngaard (1989). It can be seen that the transport term (T) is larger than the pressure term (P) by a nearly constant positive value throughout most of the CABL (i.e., for $0.1 \leq z/Z_i \leq 0.8$), which makes them approach zero at different heights; in particular, at one-third of the CABL depth, only P and B terms of Eq. (1) are different from zero. Therefore, T was empirically parameterized as

$$\mathrm{T} \approx \mathrm{P} + b\frac{w_*^2\theta_*}{Z_i}, \quad (2)$$

where $b \approx 2$.

The above empirical equation (2) is supported by Air-Mass Transportation Experiment (AMTEX) data (Lenschow et al. 1980) in the upper half of CABL. Actually, however, in the lower half of CABL, the difference be-

tween T and P is larger than $2w_*^2\theta_*/Z_i$ (that is also to say $b \geq 2$). This, according to Holtslag and Moeng (1991), might be due to measuring errors; in fact, because both T and P are difficult to measure and since P was obtained as a residual term in Lenschow et al. (1980), the outcome becomes very sensitive to the measuring errors. For these reasons, the condition $b \approx 2$ can be considered reasonable, because it is within the experiment errors.

Concerning the pressure convariance term P, Moeng and Wyngaard (1986), on the basis of LES data, resolved the pressure field into turbulence–turbulence, mean shear, buoyancy, Coriolis, and subgrid-scale components and found that buoyancy and turbulence–turbulence dominate in CABL. More specifically, they showed that the contribution of the buoyancy to the pressure gradient–potential temperature covariance $[-(1/\rho_0)(\overline{\theta\partial p/\partial z})]$ can be parameterized as one-half of the rate of direct buoyant production $[-(g/\Theta)\overline{\theta^2}]$, while the contribution of the turbulence–turbulence $(\overline{w\theta}/\tau_i)$ can be parameterized with Rotta's return to isotropy assumption, Consequently, they proposed the following modeling for P:

$$\mathrm{P} = -\alpha\frac{g}{\Theta}\overline{\theta^2} - \frac{\overline{w\theta}}{\tau_i}, \tag{3}$$

where τ_i is a return to isotropy timescale ($\tau_i = 0.5Z_i/w_*$; Holtslag and Moeng 1991), and α is a constant.

Substituting Eq. (2) and Eq. (3) into Eq. (1), Holtslag and Moeng (1991) obtained

$$\frac{\partial\overline{w\theta}}{\partial t} \approx -\overline{w^2}\frac{\partial\Theta}{\partial z} + (1-2\alpha)\frac{g}{\Theta}\overline{\theta^2} - 2\frac{\overline{w\theta}}{\tau_i} + b\frac{w_*^2\theta_*}{Z_i}. \tag{4}$$

They also adopted a turbulence within the CABL for which $\alpha = \frac{1}{2}$ (Moeng and Wyngaard 1986) that makes the buoyancy $g\overline{\theta^2}/\Theta$ disappear from Eq. (4). In quasi-steady states, Eq. (4) becomes

$$\frac{\overline{w\theta}}{\tau_i} \approx -\frac{\overline{w^2}}{2}\frac{\partial\Theta}{\partial z} + \frac{b}{2}\frac{w_*^2\theta_*}{Z_i}. \tag{5}$$

From Eq. (5), it is clear that the heat flux depends on the local downgradient transport (first term on rhs) and on a nonlocal countergradient transport (second term), which arises from the turbulent transport term (T) of Eq. (1) and is proportional to the surface heat flux (nonlocal parameterization). Just for sake of completeness, we recall that Zilitinkevich et al. (1999) noted the parameterization of the third-order moment representing the nonlocal transport term (T) was made through an algebraic combination of second-order moments, giving rise to closures that can be considered something like a pseudo-nonlocal closure in virtue of the involvement of nonlocal fearures like w_* and Z_i.

Thanks to a different formulation of Eq. (5) that reads

$$\overline{w\theta} = -K_H\left(\frac{\partial\Theta}{\partial z} - r_\theta\right), \tag{6}$$

where K_H is an eddy diffusivity and r_θ is a countergradient term, Holtslag and Moeng (1991) could compare, in a rational and clear way, the differences between the physical meaning of the countergradient term obtained by them with respect to the corresponding one obtained by Deardorff (1972). In fact, by combining Eq. (5) with Eq. (6), one obtains K_H and r_θ expressions compatible with the derivation of Holtslag and Moeng, that is,

$$\text{local downgradient,} \qquad K_H = \overline{w^2}\frac{\tau_i}{2}, \tag{7}$$

$$\text{nonlocal countergradient,} \qquad r_\theta = b\frac{w_*^2\theta_*}{\overline{w^2}Z_i}. \tag{8}$$

Differently from Holtslag and Moeng, as we already noted, Deardorff (1972) derived an equation similar to Eq. (5) by neglecting the turbulent transport (T) in Eq. (1) and parameterizing the pressure covariance P by using Eq. (3) with $\alpha = 0$. This makes use of

$$\mathrm{P} = -\frac{1}{\rho_0}\frac{\overline{\theta\partial p}}{\partial z} = -\frac{\overline{w\theta}}{\tau_D}, \tag{9}$$

where τ_D is a timescale related to the turbulence energy and a mixing length. In this case, Eq. (6), combined with the parameterization of the pressure covariance (P) of Deardorff (1972) [Eq. (9)], gives the K_H and r_θ expressions compatible with his derivation, that is,

$$\text{local downgradient,} \qquad K_H = \overline{w^2}\tau, \tag{10}$$

$$\text{local countergradient,} \qquad r_\theta = \frac{g}{\Theta}\frac{\overline{\theta^2}}{\overline{w^2}}. \tag{11}$$

From Eq. (8), the countergradient results from the third-moment transport effect, while from Eq. (11), the countergradient is related to the local buoyant production term (B) of the heat flux equation [Eq. (1)].

A detailed and thorough comparison between the countergradient terms (8) and (11) has been made by Holtslag and Moeng in their paper (1991) on the basis of turbulent quantities obtained from LES data. In the present paper, as we already said, we are interested in estimating the values of each term in Eq. (5), especially the countergradient term, by using the atmospheric data observed in the CABL of a semiarid region near Beijing, China, in 1994, and comparing them with the Holtslag and Moeng derivation.

3. Description of experimental observations

The WL-ARPDD94 field experiment in Xianghe (39°40′N, 116°59′E; 70 km southeast of Beijing), carried out in the frame of the World Laboratory Applied Research Project on Drought and Desertification, was launched in 15 August 1994 and lasted one month. The scientific and applied purposes of this experiment were the study of the dynamic and thermal characteristics of the boundary layer structure in the greater Beijing area (including the city and its rural surrounding region) in

summertime, and the record of data for research on heat and water exchanges from the soil surface and lower troposphere in the dry Beijing Plain. However, the data collected during the experiment could also provide useful information for more basic turbulence studies in convective conditions.

The observation system layout included the following.

1) Movable tower system for field observation. This 32-m tower had five platforms. On each of them, slow-response (0.1-Hz sampling rate) cup anemometers, thermometers, and hygrometers were mounted to measure average vertical profiles of wind, temperature, and humidity in the surface layer. In addition, three sets of fast-response sonic anemometers were installed at 4, 8, and 16 m to observe surface fluxes of momentum and heat. The sampling rate of all these fast-response instruments was 10 Hz.
2) PA2 Doppler sodar. This sodar, manufactured by Remtech (France), was used to obtain vertical profiles of mean wind speed and direction and of variance of its vertical component below 1000 m. It is a phased-array system with 196 individual speakers and receivers, using five different frequencies around 2250 Hz and a pulse length of 200 ms for each frequency. The tilted beams have an angle of 30° to the vertical.

   The instrument technical specifications are the following. Minimum altitude sampled: 50 m; vertical sampling: 20 m; accuracy: 3% on horizontal wind speed, 3° on wind direction and 10–20 cm s^{-1} on vertical wind speed. Averaging time: 30 min.
3) Radio Acoustic Sounding System (RASS) manufactured by Airone (Italy), with automatic compensation for moisture, to measure the vertical profiles of absolute air temperature below 1000 m (Bonino and Trivero 1985). The instrument's technical specifications are the following. Radio frequency: 415 MHz; acoustic frequency: 300 Hz; minimum altitude sampled: 70 m; vertical sampling: 20 m; accuracy: 0.2°C (for 30-min average soundings). In the software of our radio acoustic sounding system there is also a floor of signal-to-noise ratio below which all data are discarded.

In addition, other instruments designed for the purpose of the Xianghe experiment to assess the surface energy and water balance were also deployed. They were the following.

1) LAP-3000 Profiler System. This system, based on radio and acoustic wave interaction and manufactured by Radian (United States), was used to obtain data of wind and virtual temperature vertical profiles up to 4 km. The instrument's technical specifications are the following. Radio frequency (pulsed transmission): 915 MHz; acoustic frequency (continuous transmission): 2 kHz; minimum altitude sampled: 100 m; range of wind profile: 2–5 km; vertical sampling of wind profile: 60–400 m; accuracy: <1 m s^{-1} on wind speed and $<10°$ on wind direction; range of virtual temperature profile: 1–2 km; vertical sampling of temperature profile: 60 m; accuracy: 1°C.
2) Net solar radiation to measure the radiative energy balance.
3) Underground slow-response sensors to measure vertical profiles of temperature and humidity in the soil.

4. Profile of sensible heat flux

In order to estimate the value of each term in Eq. (5), the profiles of sensible heat flux and of vertical velocity variance are necessary. However, in our observation, there is not any direct observation of the sensible heat flux profile but only of the vertical profile of the vertical velocity variance, measured by Doppler shift of the acoustic sounder (PA2) with an accuracy of about 25% (as shown in Fig. 6). In principle one could try to calculate correlated products $\overline{wT}$ of instantaneous values of vertical velocity measured by the Doppler sodar PA2 and temperature measured by the RASS. This would allow one to obtain sensible heat fluxes at different heights in the CABL. Unfortunately, as we shall discuss in more detail later in section 6, instantaneous observation of T are affected by large errors, depending also on the value of w, and this makes any estimate of heat flux meaningless. In such a situation, it has been a force majeure to attempt to estimate the vertical distribution of sensible heat flux by resorting to similarity theory and indirect observations. From similarity theory (Panofsky and McCormick 1960; Panofsky et al. 1977; Panofsky 1978), sensible heat flux and vertical velocity variance are related to each other by the approximate equation:

$$\overline{w^2} \approx A\left[z\left(-\overline{uw}\frac{du}{dz} + \delta\frac{g}{\theta}\overline{w\theta}\right)\right]^{2/3}. \qquad (12)$$

In a well-mixed layer with moderate wind (less than 3 m s^{-1}) and at heights z large enough to allow use of the free-convection assumption, the mechanical production is negligible (Coulter and Weseley 1980) and the above equation can be simplified to

$$\overline{w^2} \approx \alpha\left(z\frac{g}{\theta}\overline{w\theta}\right)^{2/3}, \qquad (13)$$

where $\alpha = A\delta^{2/3} \approx 1.4$ (according to Caughey and Readings 1994; McBean and McPherson 1976). Equation (13) shows that a plot of $(\overline{w^2})^{3/2}/z$ versus z can provide an estimate of the heat flux profile in mixed layers. Therefore, from vertical velocity variance measured by PA2 (over an averaging time of 30 min), the heat flux profile can be determined.

The issue of reliability of $\overline{w^2}$ Doppler sodar observations is quite controversial. Gaynor et al. (1983) presented preliminary results of a comparison among dif-

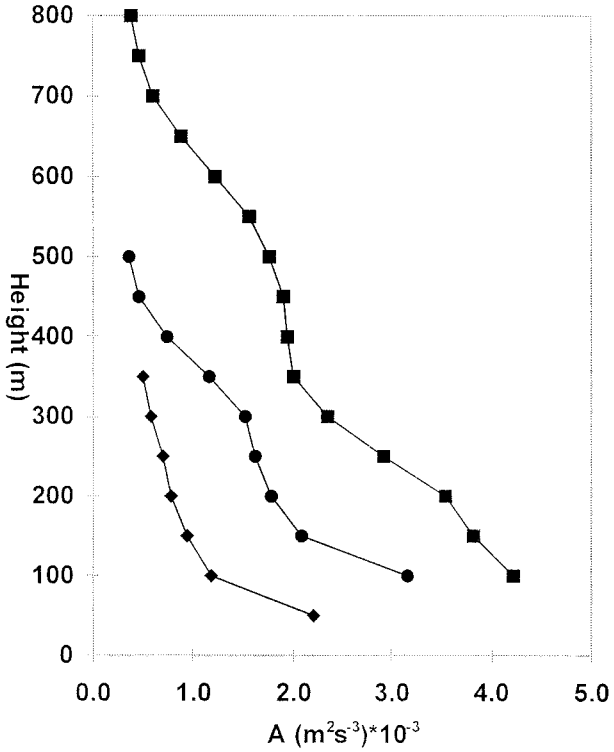

FIG. 2. Vertical profiles of $A = (\overline{w^2})^{3/2}/z$ in Xianghe measured by PA2 on 25 Aug 1994. Line with circles is for 1100 LST; line with squares, 1230 LST; line with diamonds, 1500 LST. Numbers on the abscissa must be multiplied by 10^{-3}. Profile of 1500 LST is more nearly quasi-stationary while the other two are still affected by the morning transition.

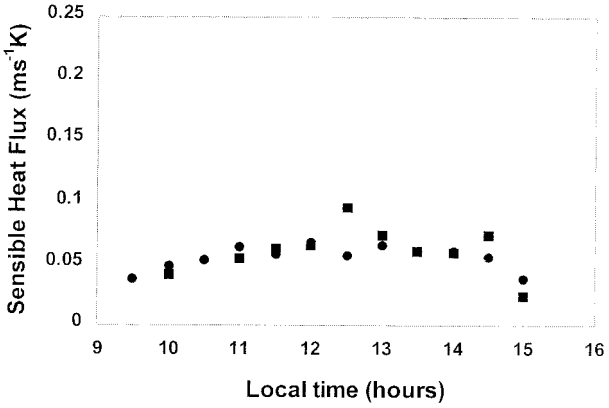

FIG. 3. A daytime variation of surface heat flux on 5 Sep 1994 in Xianghe. Squares are heat flux at 12 m, extrapolated from PA2 estimates. Circles are averaged heat flux calculated from surface observation data collected with two sonic anemometers at 8 and 16 m.

ferent sodar system and sonic anemometers at the 200-m level of the BAO tower, aimed at assessing the ability of sodar to measure the standard deviation of the vertical component σ_w; they showed that the scatter of sodar data was large for all sodars, but at least it was evenly distributed around the 1:1 line in daytime. Thomas and Vogt (1993), from the results of an intercomparison of a sonic anemometer and a Doppler sodar similar to the one used by us in Xianghe, found that the sodar sounding was a reliable technique to determine, besides the mean field, also atmospheric turbulence data like σ_w. More recently, Peters et al. (1998) could obtain vertical profiles of σ_w for different classes of stability conditions up to 270 m and concluded that, in addition to profiles of mean values, Doppler sodars can also measure turbulent parameters with adequate quality. On the contrary, Seibert and Langer (1996) reported a negative bias in the sodar measurement of σ_w under convective conditions.

An obvious consequence of the above-mentioned method for assessing heat flux from $\overline{w^2}$ is that the outcome of testing of Eq. (5) depends on the performance of Eq. (13) through the CABL. As already said, we did not have any way to validate the whole vertical profiles of heat flux estimated by PA2 with direct local observation; however, it was possible to do this near the surface, where the turbulent heat flux could be evaluated from the sonic anemometer readings through the application of the eddy correlation method.

In a well-mixed layer, $\partial\Theta/\partial z \approx 0$ and heat flux decreases linearly with height up to the base of the transition layer mainly during the morning, when convection is shallow (Weill et al. 1980). Under these circumstance, Eq. (13) can be written as

$$\frac{(\overline{w^2})^{3/2}}{z} \approx \alpha^{3/2}\frac{g}{\theta}\left[(\overline{w\theta})_0\left(1 - \frac{z}{Z'}\right)\right], \qquad (14)$$

where Z' is the height at which the heat flux vanishes by linear extrapolation. We point out that the height Z' does not coincide with the real height at which the heat flux becomes zero, even if it is close to it (Fig. 1 of Weill et al. 1980). From the above equation, $(\overline{w^2})^{3/2}/z$ also has a nearly linear course with height z. Figure 2 shows a few examples of vertical profiles of $(\overline{w^2})^{3/2}/z$. The profile of 1500 LST (local standard time) is really stationary, while the other two (at 1100 LST and 1230 LST) are still affected by the morning transition.

By extrapolating the profiles at a height of 12 m above the surface, we get the surface heat flux from Eq. (14). Figure 3 shows a daytime variation of heat flux estimated by PA2 and that measured by the sonic anemometers installed on the tower at 8 and 16 m. The surface heat flux estimated by this method showed a good agreement with the one calculated by the eddy correlation method with sonic anemometer data at the surface in weak wind conditions.

Figure 4 shows the comparison of surface heat fluxes obtained by extrapolating all available $(\overline{w^2})^{3/2}/z$ profiles from PA2 with those measured by sonic anemometers in convective conditions with wind speed less than 3 m s^{-1}. The regression equation reads $y = 0.7576x + 0.0139$, with a correlation coefficient of 0.84 (y = PA2 heat flux; x = sonic anemometer heat flux, in units of

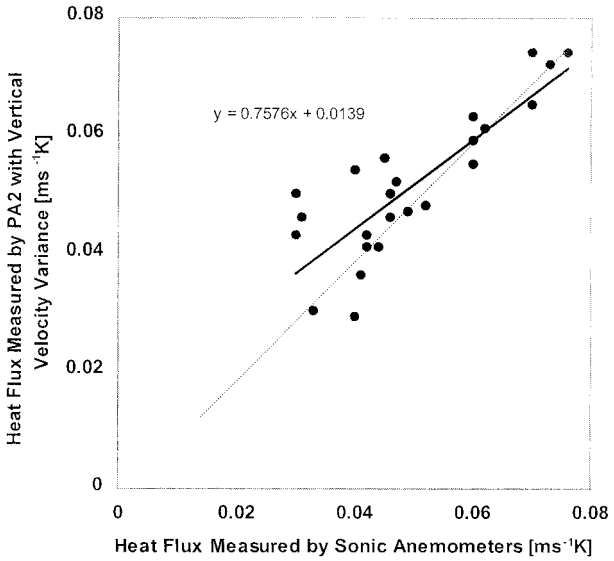

FIG. 4. Comparison among all couples of surface heat flux simultaneously estimated at 12 m by PA2 and sonic anemometers during moderate wind conditions (less than 3 m s^{-1}) in Xianghe (dashed line represents the 1:1 line; continuous line represents the regression line).

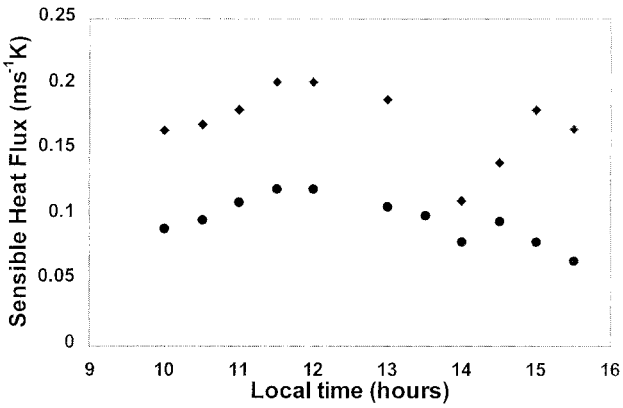

FIG. 5. A daytime variation of surface heat flux on a strong wind day (10 Sep 1994) in Xianghe. Diamonds are heat flux at 12 m, extrapolated from PA2 estimates. Circles are averaged heat flux calculated from surface observation data collected with two sonic anemometers at 8 and 16 m.

m s^{-1} K), and shows that their relative average difference is about 10%. Furthermore, it shows that sodar surface heat flux measurements overestimate small in situ surface heat fluxes measured by sonic anemometers, as a consequence of the corresponding similar overestimated σ_w (Beyrich and Kotroni 1993; see also section 5). Nevertheless, even if our statistic is poorer, the scatter of our data seems to be of the same order of magnitude as, or lower than, that obtained by Angevine et al. (1998) from a boundary layer wind profiler. As Eq. (12) shows, the vertical velocity variance measured by PA2 includes both mechanical production and buoyancy production, while in order to estimate sensible heat flux vertical profile, we used Eq. (14), in which the mechanical production term does not appear. On strong wind days, the mechanical production cannot be neglected. So the PA2 might overestimate the surface heat flux in this situation. Figure 5 shows an example of this, recorded on a strong wind day (10 September 1994), when the surface wind velocity was between 6 and 8 m s^{-1} (half-hour averages). In this case, the difference between the two estimations can be as large as 100%. This fact proves, from another point of view, that the vertical velocity variance measured by PA2 can be considered a reliable parameter to be used for estimating heat flux profiles in mixed layers of CABL only under moderate wind conditions.

5. Normalized vertical velocity variance

Under low-wind and convective conditions, when the ratio u_*^2/w_*^2 is typically $O(10^{-1})$, the profiles of vertical velocity variance (measured by half-hour means of PA2 soundings) can be normalized by using only the mixing height Z_i (based on temperature profile measured by the RASS) and the vertical velocity scale w_* (measured by sonic anemometers) (Lenschow et al. 1980).

Ten profiles of vertical velocity variance chosen from our observation period when both PA2 and RASS performed particularly well at the same time (so that the mixing heights could be clearly identified from the temperature profiles detected by RASS) have then been normalized with Z_i and w_* scales. Table 1 lists the dates and local times of these 10 profiles, together with some typical scales of the boundary layer measured by the fast-response ultrasonic anemometers.

Because most profiles matching the above conditions were detected after rain episodes, the ground surface was wet. Under these conditions, the solar energy that gets to the earth surface is also used for evaporation, so that the sensible heat flux is reduced and the mixing heights are consequently low. After normalizing the vertical velocity variance with w_*^2, we obtained the results shown in Fig. 6. The experiment data are well fitted by the relationship

$$\frac{w^2}{w_*^2} = 1.5\left(\frac{z}{Z_i}\right)^{2/3}\left(1 - 0.9\frac{z}{Z_i}\right). \qquad (15)$$

Since our normalized variances ($\overline{w^2}/\overline{w_*^2}$) refer to shallow convection over homogeneous terrain, it can be interesting to compare their vertical distribution all through the depth of CABL with those of different situations. For this reason, the ($\overline{w^2}/\overline{w_*^2}$) vertical profiles observed in our experiment at Xianghe have been compared with the ($\overline{w^2}/\overline{w_*^2}$) vertical profiles obtained in the already quoted AMTEX experiment (Lenschow et al. 1980), where convection was generated by advection, and with the ($\overline{w^2}/\overline{w_*^2}$) profiles obtained in the LES experiment (Moeng and Wyngaard 1989), where pure convection was assumed. The comparison has been ex-

TABLE 1. Boundary layer parameters.

Local time and date (LST)	Z_i(m)	U (m s^{-1}) at 12 m	u_* (m s^{-1})	W_* (m s^{-1})	θ_* (K)	$\overline{w\theta_0}$ (m s^{-1} K) $\times$ 1000	τ_i (s)
1130 25 Aug	510	1.0	0.09	0.92	0.50	46	279
1230 25 Aug	510	1.4	0.12	0.90	0.49	44	283
1330 25 Aug	480	1.8	0.14	0.86	0.48	41	278
1230 30 Aug	450	2.0	0.14	0.96	0.63	60	235
1100 5 Sep	600	2.6	0.13	1.06	0.57	60	284
1500 5 Sep	660	2.8	0.47	0.95	0.42	40	347
1000 7 Sep	480	2.2	0.22	0.82	0.43	35	293
1030 7 Sep	390	2.5	0.35	0.87	0.59	51	225
1200 7 Sep	720	2.5	0.33	1.04	0.46	48	346
1230 7 Sep	620	2.4	0.36	1.00	0.49	49	311

tended as far as $z/Z_i = 1$, in order to match the same range considered by AMTEX and LES experiments.

The comparison of our results with the AMTEX data in Fig. 6, notwithstanding a noticeable scatter corresponding to an error of about 25%, shows that qualitatively the curves are similar, apart from a little overestimate, while LES data sensibly underestimate both our and AMTEX observations.

On one hand, LES data were obtained by adopting a normalizing factor w_* of 2 m s^{-1}, while our observed w_* is only O(1 m s^{-1}), and this could partly explain why simulated LES data underestimate our observed nondimensional data. On the other hand, sodar σ_w measurements overestimate small in situ values, as it is already known from other comparisons (Beyrich and Kotroni 1993). Furthermore, our data refer to situations in which the vertical velocity field could also be influenced by baroclinicity effects, likely to occur in weather conditions where rainfall episodes alternated with sunny and unperturbed conditions.

6. Experimental evaluation of each term of Eq. (5)

In this section we focus our attention only on the evaluation of the terms appearing on both sides of Eq. (5), and check its balance, for two reasons. First, Eq. (5) represents a more advanced and physically consistent approach to the modeling of turbulent transport of heat than the classic approach of Deardorff [(1972), Eq. (11)]. Second, no direct observation of $\overline{\theta^2}$ was available

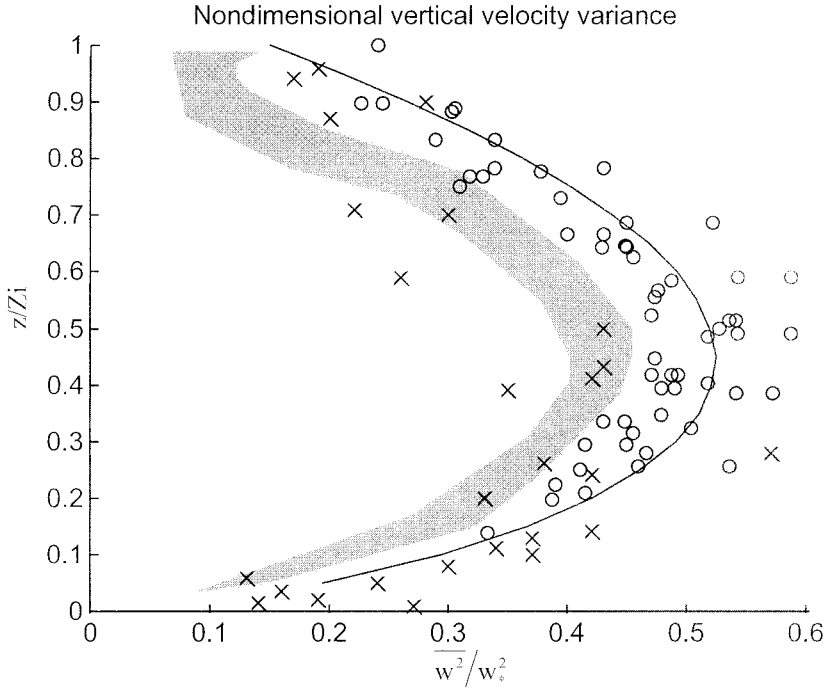

FIG. 6. Comparison among normalized vertical velocity variances as a function of relative height in the CABL. Circles are Xianghe data, crosses are AMTEX data, and shaded area shows LES data.

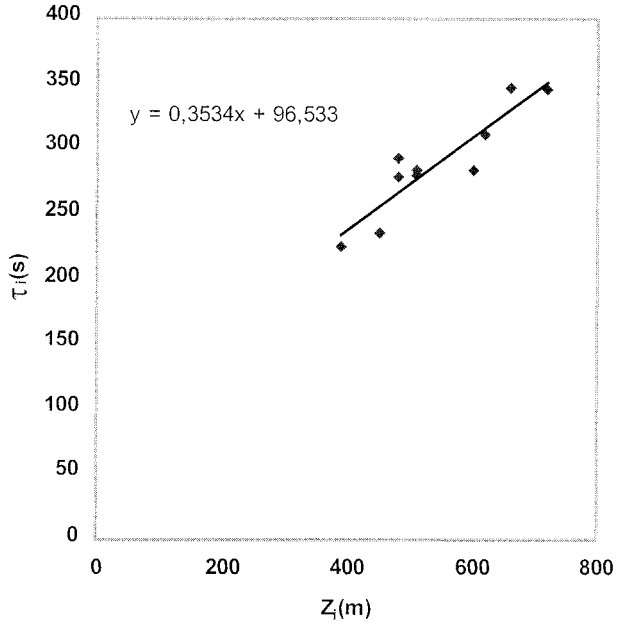

FIG. 7. Plot of the return-to-isotropy timescale τ_i (diamonds) as a function of the CABL depths found in the Xianghe experiment (continuous line represents the regression line).

to us, which prevented us from evaluating the Deardorff local countergradient term [Eq. (11)]. Equation (5) has been evaluated in the range of (dimensionless) heights $0.1 \leq z/Z_i \leq 0.8$, where the turbulent transport term T is larger than P by a nearly constant value and can be parameterized according to Eq. (2).

In order to obtain an overall test of Eq. (5), filtered from the day-to-day variability of atmospheric stability conditions, the experimental estimates of the three terms of Eq. (5) as a function of the relative height, presented in this section, represent their average values evaluated from the 10 episodes of the Xianghe field experiment selected according to the criteria discussed in section 5. The term $\overline{w\theta}/\tau_i$ at the lhs of Eq. (5), representing the sensible heat flux divided by the "return-to-isotropy timescale τ_i," has been assessed by using Eq. (13), where $\overline{w^2}$ comes from the following regression equation of the normalized vertical velocity variance.

$$\frac{w^2}{w_*^2} = 1.46\left(\frac{z}{Z_i}\right)^{2/3}\left(1 - 0.9\frac{z}{Z_i}\right). \qquad (15')$$

Equation (15′) is based on our observation limited to the range of dimensionless heights $0.1 \leq z/Z_i \leq 0.8$. As a matter of fact, Eq. (15′) turned out to be almost the same as Eq. (15).

The time scale $\tau_i = 0.5Z_i/w_*$ (valid in the middle part of the CABL; Holtslag and Moeng 1991) was estimated with the measurement of the RASS and sonic anemometer. Figure 7, plotting the return-to-isotropy timescale τ_i as a function of the CABL depths of our experiments (Table 1), shows that τ_i actually depended on Z_i (regression equation reads $\tau_i = 0.3534Z_i + 96.533$), so revealing that the influence of the height near the boundaries was present, as in LES.

The countergradient term [the nonlocal convective transport term, that is, the second term at the rhs of Eq. (5), coming from the turbulence transport term] is proportional to the surface heat flux through the convective velocity scale w_*, measured by the sonic anemometers, and to the inverse of the CABL depth (Z_i), corresponding to the height of temperature inversion capping the convective layer and measured by the RASS. On this subject, the temperature profile recorded by our RASS are half-hour averages of subsequent instantaneous soundings, each of them validated by a floor of signal-to-noise ratio (see section 3c); this reduces to a large extent the uncertainties inherent in single measurements $O(1°C)$ due to fluctuations of vertical speed (w) (updrafts and downdrafts almost balance each other out over 30 min). Validation tests carried out during calibration experiments (Bonino et al. 1981) showed that the typical accuracy of temperature readings obtained by a RASS of the same type of the one operating at Xianghe is $O(10^{-1}\ °C)$, so that the depth of CABL can be reliably assessed with this method. Figure 8 shows the observed vertical profiles of the heat flux (line with circles) and the countergradient term (line with squares) as a function of the dimensionless depth z/Z_i. The countergradient term is constant with height; it crosses the heat flux profile at the height of about $0.45z/Z_i$. It clearly appears that the countergradient term takes the main role in convective conditions, mainly in the middle of the CABL.

For the estimate of the local gradient term [first term at the rhs of Eq. (5)], the profile of the vertical potential temperature gradient must also be known in addition to the profile of the vertical velocity variance. From our observation of vertical profiles of T with the RASS, the profiles of the vertical equivalent potential temperature (θ) gradient were obtained and normalized with Z_i and θ_* (Lenschow et al. 1980). It is beyond any doubt that basic versions of RASS equipment measure something that is a close approximation to the virtual temperature (T_v). However, our RASS (see Bonino and Trivero 1985) was equipped with a device and software automatically compensating its readings for air moisture, so bringing its observation very close to the absolute temperature (T). Furthermore, even in the absence of compensation for moisture, the difference between dT/dz and dT_v/dz in the CABL is expected to be negligible (even when the difference between T and T_v is not negligible), on account of the small temperature lapse rates (order of <1 K/100 m) and the uniform vertical distributions of moisture, which are both typical of CABL (at any rate, in prevailing condition of the convective boundary layer, this difference is less than 1.8×10^{-4} K m^{-1} in a saturated CABL at 308 K). For this reason, all equations have been written in potential temperature (θ). For this reason, our equations will be written in terms of Θ and

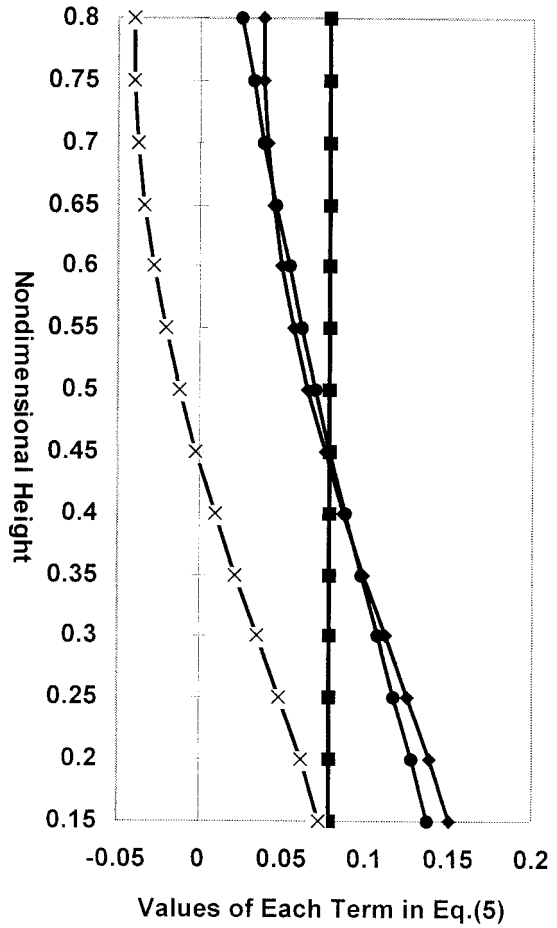

FIG. 8. Experimental values of each term of Eq. (5) as a function of z/Z_i. Line with squares is the countergradient term. Line with crosses is the local, or downgradient, term. Line with diamonds is sensible heat flux divided by the timescale τ_i ($\overline{w\theta}/\tau_i$) resulting from combination of measured downgradient and countergradient terms [Eq. (5)]. Line with (solid) circles is directly measured sensible heat flux divided by the timescale τ_i ($\overline{w\theta}/\tau_i$).

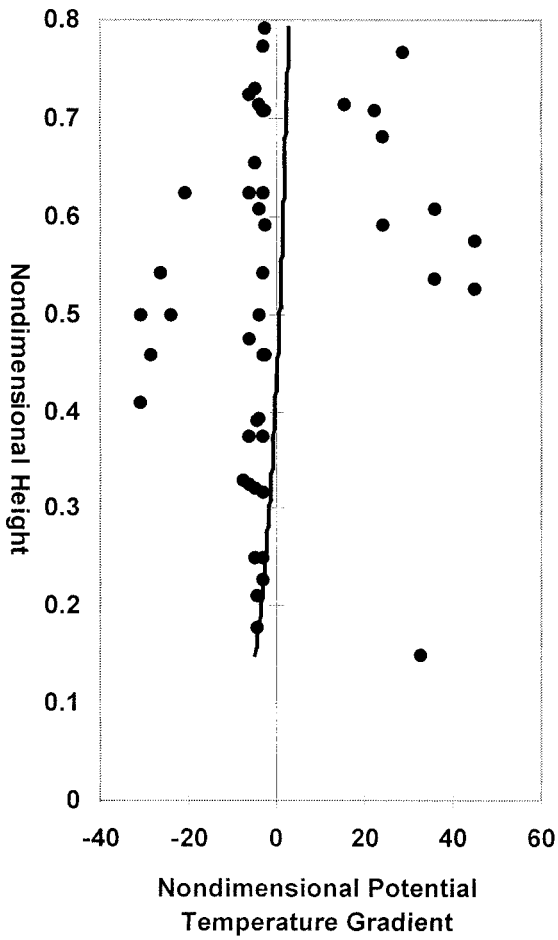

FIG. 9. Vertical profile of normalized $[(Z_i/\theta_*)/(\partial\theta/\partial z)]$ vertical potential temperature gradient (the dimensionless value of 10 on the abscissa corresponds to $\partial\theta/\partial z = 8 \times 10^{-3}$ K m^{-1}).

θ instead of Θ_v and θ_v. Figure 9 shows the result. The continuous line is the best fit of the observed data, which appear more scattered in the upper region of the CABL. This scatter is also due to the fact that we have fitted the overall dataset, obtained in a different stability condition. However, as the vertical gradient of potential temperature in Fig. 9 has been normalized with θ_*/Z_i, a quantity that is typically $O(5 \times 10^{-2}$ K m$^{-1})$, the scatter of data in Fig. 9 seems too large (for instance, the dimensionless value of 10 on the abscissas corresponds to only $\partial\theta/\partial z = 8 \times 10^{-3}$ K m^{-1}). The result of the fitting is

$$\frac{Z_i}{\theta_*}\frac{\partial\Theta}{\partial z} = 4.6\ln\left(\frac{z}{Z_i}\right) + 3.8 \qquad 0.15 \le \frac{z}{Z_i} \le 0.80. \quad (16)$$

As for comparison, AMTEX data (Lenschow et al. 1980) determined the normalized vertical potential temperature gradient as

$$\frac{Z_i}{\theta_*}\frac{\partial\Theta}{\partial z} = 1.4 = \text{constant}. \quad (17)$$

Finally, Eq. (16) allows the calculation of the local gradient term. It is shown in Fig. 8 (line with crosses).

If the local gradient term and the countergradient term estimated as above-described are combined, we get the line (with squares) representing the vertical profile of the term $\overline{w\theta}/\tau_i$ evaluated through Eq. (5). As Fig. 8 shows, it exhibits a good agreement with the vertical profile of directly measured values of term $\overline{w\theta}/\tau_i$ (line with circles), with an average difference around 1%.

7. Conclusions

Holtslag and Moeng proposed in 1991 a simple and physically consistent version of the turbulent heat flux equation in the convective atmospheric boundary layer. The most salient feature of their new approach was that it did not neglect the third-order moment, or transport term, that was parameterized as a function of a pressure

covariance term and a nonlocal convective term. In this paper, we have presented and discussed the results of an experimental evaluation of the Holtslag and Moeng equation of turbulent heat flux where each term at both sides of the equation has been evaluated by using independent observations gathered from a field experiment on the convective boundary layer (WL-ARPDD94 Experiment—Xianghe, China).

In order to obtain an overall test of the Holtslag and Moeng equation filtered from the day-to-day variability of atmospheric conditions, we used the overall dataset referring to CABL conditions with moderate horizontal wind.

A satisfactory agreement has been found between measured right-hand and left-hand sides of the equation, in a range of conditions including also moderate values of turbulent heat flux and very low speeds of surface wind. This result appears particularly interesting and promising also from the application standpoint, in view of the ability of this model to be generalized to the description of diffusion and transport of scalar fluxes (like moisture or airborne contaminants) at the surface and at the top of the convective atmospheric boundary layer.

Acknowledgments. The authors thank Dr. Renato Forza from the Department of General Physics of Turin University and Dr. Aiguo Li from the Institute of Atmospheric Physics of the Chinese Academy of Sciences for their professional job to ensure the advanced remote instrument operation with a high quality of data.

REFERENCES

Angevine, W. M., P. S. Bakwin, and K. J. Davis, 1998: Wind profiler and RASS measurements compared with measurements from a 450-m-tall tower. *J. Atmos. Oceanic Technol.,* **15,** 818–825.

Beyrich, F., and V. Kotroni, 1993: Estimation of surface stress over a forest from sodar measurements and its use to parameterize the stable boundary-layer height. *Bound.-Layer Meteor.,* **66,** 92–103.

Bonino, G., and P. Trivero, 1985: Automatic turning of Bragg condition in a radio-acoustic system for PBL temperature profile measurement. *Atmos. Environ.,* **10,** 973–978.

——, P. P. Lombardini, A. Longhetto, and P. Trivero, 1981: Radio-acoustic measurements of fog capping thermal inversion. *Nature,* **920,** 121–123.

Caughey, S. J., and C. J. Readings, 1994: Vertical components of turbulence in convective conditions. *Advances in Geophysics,* Vol. 18A, Academic Press, 125–130.

Coulter, R. L., and M. L. Weseley, 1980: Estimates of surface heat flux from sodar and laser scintillation measurements in the unstable boundary layer. *J. Appl. Meteor.,* **19,** 1209–1222.

Cuijpers, J. W. M., and A. A. M. Holtslag, 1998: Impact of skewness and nonlocal effects on scalar and buoyancy flux in convective boundary layers. *J. Atmos. Sci.,* **55,** 151–162.

Deardorff, J. W., 1966: The counter-gradient heat flux in the lower atmosphere and in the laboratory. *J. Atmos. Sci.,* **23,** 503–506.

——, 1972: Theoretical expression for the counter-gradient vertical heat flux. *J. Geophys. Res.,* **77,** 5900–5904.

Ebert, E. E., U. Schumann, and R. B. Stull, 1989: Nonlocal turbulent mixing in the convective boundary layer evaluated from large-eddy simulation. *J. Atmos. Sci.,* **46,** 2178–2207.

Gaynor, J. E., J. C. Kaimal, and T. J. Lockhart, 1983: Evaluation of wind parameters measured by four acoustic Doppler systems. Preprints, *Fifth Symp. Meteorological Observations and Instrumentation,* Toronto, ON, Canada, Amer. Meteor. Soc., 488–491.

Holtslag, A. A. M., and C.-H. Moeng, 1991: Eddy diffusivity and countergradient transport in the convective atmospheric boundary layer. *J. Atmos. Sci.,* **48,** 1690–1698.

Lenschow, D. H., J. C. Wyngaard, and W. T. Pennell, 1980: Mean-field and second-moment budgets in a baroclinic, convective boundary layer. *J. Atmos. Sci.,* **37,** 1313–1326.

McBean, G. A., and J. I. McPherson, 1976: Turbulence above Lake Ontario: Velocity and scalar statistics. *Bound.-Layer Meteor.,* **10,** 181–107.

Moeng, C.-H., and J. C. Wyngaard, 1986: An analysis of closures for pressure-scalar covariances in the convective boundary layer. *J. Atmos. Sci.,* **43,** 2499–2513.

——, and ——, 1989: Evaluation of turbulent transport and dissipation closures in second-order modeling. *J. Atmos. Sci.,* **46,** 2311–2330.

Panofsky, H. A., 1978: Matching in the convective planetary boundary layer. *J. Atmos. Sci.,* **35,** 272–276.

——, and R. McCormick, 1960: The spectrum of vertical velocity near the surface. *Quart. J. Roy. Meteor. Soc.,* **86,** 495–503.

——, H. Tennekes, D. H. Lenschow, and J. C. Wyngaard, 1977: The characteristics of turbulent velocity components in the surface layer under convective conditions. *Bound.-Layer Meteor.,* **11,** 335–361.

Peters, G., B. Fischer, and H. J. Kirtzel, 1998: One-year operational measurements with a sonic anemometer–thermometer and a Doppler sodar. *J. Atmos. Oceanic Technol.,* **15,** 18–28.

Seibert, P., and M. Langer, 1996: Deriving characteristic parameters of the convective boundary layer from sodar measurements of the vertical velocity variance. *Bound.-Layer Meteor.,* **81,** 11–22.

Thomas, P., and S. Vogt, 1993: Intercomparison of turbulence data measured by sodar and sonic Anemometers. *Bound.-Layer Meteor.,* **62,** 353–359.

Troen, I., and L. Mahrt, 1986: A simple model of the atmospheric boundary layer; Sensitivity to surface evaporation. *Bound.-Layer Meteor.,* **37,** 129–148.

Weill, A., C. Klapisz, B. Strauss, F. Baudin, and C. Jaupart, 1980: Measuring heat flux and structure functions of temperature fluctuations with an acoustic Doppler sodar. *J. Appl. Meteor.,* **19,** 199–205.

Wyngaard, J. C., and J. C. Weil, 1991: Transport asymmetry in skewed turbulence. *Phys. Fluids,* **A3,** 155–162.

Zilitinkevich, S., V. M. Gryanik, V. N. Lykossov, and D. V. Mironov, 1999: Third-order transport and nonlocal turbulence closure for convective boundary layers. *J. Atmos. Sci.,* **56,** 3463–3477.